

Finite Elements Model Co-Simulation of an Induction Motor Drive for Traction Application

Lino Di Leonardo
*Department of Industrial and Information Engineering and
Economics*
University of L'Aquila
L'Aquila
lino.dileonardo@univaq.it

Mircea Popescu
Motor Design Ltd.
Wrexham, United Kingdom
mircea.popescu@motor-design.com

Marco Tursini
*Department of Industrial and Information Engineering and
Economics*
University of L'Aquila
L'Aquila
marco.tursini@univaq.it

Marco Villani
*Department of Industrial and Information Engineering and
Economics*
University of L'Aquila
L'Aquila
marco.villani@univaq.it

Abstract— This paper presents the results obtained by the finite elements model co-simulation technique in the transient analysis of an electric drive for advanced traction applications. The case study refers to a 200kW induction motor drive designed for a premium electric vehicle in the frame of the Horizon 2020 “ReFreeDrive” project (Rare earth Free e-Drives featuring low cost manufacturing). The transient performance and the operating limits are evaluated when a field-oriented control strategy based on the lumped parameters model of the machine is used. The co-simulation involves the ANSYS/Simplorer and MATLAB/Simulink environments. The finite element motor model developed in ANSYS is controlled by the rotor flux-oriented controller with axes decoupling built in Simulink. A lumped parameters motor model is also derived to design the control parameters and implemented in Simulink for comparison respect to the co-simulation approach. The results highlight the influence of the controller detuning for the correct prediction of the voltage limit operation at steady state.

Keywords— *Electromagnetic transients, Finite element analysis, Traction motors, Induction motors, Motor drives, Power system simulation*

I. INTRODUCTION

Due to the dynamic nature of the application, the transient analysis of the motor-drive systems proposed in the emerging area of Electric Vehicles (EV) is indubitably important, [1][2].

Induction motors and Permanent Magnet (PM) synchronous motors are currently considered the better solutions for traction of EV, [3][4]. Respect to PM synchronous motors, Induction Motors (IMs) can allow for a better average efficiency in variable load conditions and easier flux-weakening capability useful for speed range extension thanks to the absence of the need for field weakening current. Moreover, the absence of rare earth magnets ensures the industrial feasibility for mass production, focused on the low cost of the manufacturing technologies, [5]. Field-oriented control combined with optimization strategies allows to reach the maximum performances that induction motors can

provide, and dynamics simulation is a relevant step to evaluate the drive capability before prototyping, [6][7].

Until today, Lumped Parameters (LP) models are used to evaluate the transient performance of electrical drives, [8]. They consist in a set of differential non-linear equation with (generally) constant parameters, and allow for computation of electrical (currents, voltages and fluxes) and mechanical (torque and speed) quantities with small calculation times still by using ordinary computers, with obvious advantages.

Since many years, the Finite Elements Method (FEM) is used in the electromagnetic design of motors and the Finite Elements Analysis (FEA) is considered to this day the most accurate method available to predict the performance of electric machines. It allows to look at not negligible phenomena, such as nonlinear magnetization characteristics and cross-coupling effects, usually not accounted in LP models, [9]. In particular, by “transient” application to evaluate the induction currents in the bars, FEA permits the steady-state and dynamic electromagnetic calculation of induction motor.

The need to simulate the entire drive, i.e. motor, power converter and control, considering the interactions between them, has led the software packages specialized in such different areas to provide on-the-run interfacing mechanisms between them, i.e. co-simulations. This is the case of the Simplorer/Maxwell - MATLAB/Simulink (SiM2SiM) interface, available since early 2000s, which allowed to link power electronics’ simulation in Simplorer and FEM motor models developed in ANSYS Maxwell® with controller’s simulation in Simulink. Unfortunately, the calculation times in co-simulation approaches can be prohibitive, especially when Pulse Width Modulated (PWM) inverter are involved. Simulation times in the range of less than one second may need several days to run on today’s computers, [10]. This requires a particular care in the choice of the time step-size and some simplification in power converter simulation. Nevertheless, co-simulation offers the opportunity for new

insights and developments related to both motor design and control. It becomes possible to evaluate the effects of motor's non-linearities on the control and to identify the related adjustments, [11][12][13].

This paper uses the co-simulation Simplorer/Simulink to analyse the performances of a 200kW induction motor designed for the traction of a high class EV. The FEM motor model developed in ANSYS Maxwell® is controlled by the rotor flux-oriented controller with axes decoupling built in MATLAB Simulink. The goal is to evaluate the effect of a field-oriented control strategy based on the usual LP model on the dynamic performance of the “actual” machine, that is simulated by its FEM model. An ideal space-vector modulated inverter is considered to achieve a viable calculation time. An exhaustive test case is considered, which includes an initial magnetization period followed by a fast speed transient toward rated speed and load torque conditions. A LP motor model is also implemented in Simulink and comparison results with the FEM model are presented, both with the controller “in loop” and “out loop”. The study highlights the different behaviours of the two motor models during transients, and the influence of the controller detuning for the correct prediction of the voltage limit operation at steady state.

The paper is organized as follows: Section II refers to the induction motor for traction application, its lumped parameters and FEM models are presented; Section III presents the rotor flux-oriented controller with axes decoupling; the co-simulation structure with LP and FEM models' comparison is described in Section IV; finally, results are presented and discussed in Section V.

II. MOTOR DESCRIPTION

Fig. 1 shows the cross section and main geometric data of the three-phase IM considered in this study, while its main data are summarized in TABLE I.

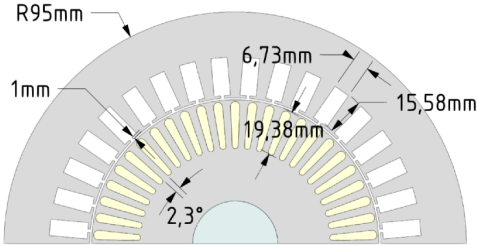


Fig. 1. Cross section and main geometric data of the IM

TABLE I. MAIN MOTOR DATA

Main motor data	
Rated power	200 kW
Rated speed	6000 rpm
Number of poles	4
Number of stator slots	36
Number of rotor bars	50
Outer / Inner stator diameter	190 mm / 119,6 mm
Outer / Inner rotor diameter	118 mm / 40 mm
Stack length	160 mm

This motor has been developed in the frame of the Horizon 2020 project ReFreeDrive “Rare earth Free e-Drives featuring low cost manufacturing” as the traction engine of high power 200kW electrical vehicles.

Key points of the design have been: 1) the cost reduction through the minimization of the motor size; 2) an optimized shape of the windings by hairpin technology, which permits to have a high efficiency (more than 94% considering WLTP class 3 drive cycle) due to lower losses and more efficient heat management although the AC winding losses due to high frequency skin and proximity effects, [14].

A. Lumped parameters model

The IM has been simulated by using the α - β lumped parameters model, where the machine is represented in terms of the equivalent two-phase circuits in the stator-aligned reference frame. By assuming the stator currents and rotor fluxes as state variables, the differential model is given by:

$$\frac{dI_{s\alpha}}{dt} = -\frac{1}{T_i}I_{s\alpha} + \frac{K_r}{\sigma L_s T_r}\Psi_{r\alpha} + \omega_r \frac{K_r}{\sigma L_s}\Psi_{r\beta} + \frac{V_{s\alpha}}{\sigma L_s} \quad (1)$$

$$\frac{dI_{s\beta}}{dt} = -\frac{1}{T_i}I_{s\beta} + \omega_r \frac{K_r}{\sigma L_s}\Psi_{r\alpha} + \frac{K_r}{\sigma L_s T_r}\Psi_{r\beta} + \frac{V_{s\beta}}{\sigma L_s} \quad (2)$$

$$\frac{d\Psi_{r\alpha}}{dt} = \frac{M}{T_r}I_{s\alpha} - \frac{\Psi_{r\alpha}}{T_r} - \omega_r \Psi_{r\beta} \quad (3)$$

$$\frac{d\Psi_{r\beta}}{dt} = \frac{M}{T_r}I_{s\beta} - \omega_r \Psi_{r\alpha} - \frac{\Psi_{r\beta}}{T_r} \quad (4)$$

where $\Psi_{r\alpha}, \Psi_{r\beta}, I_{s\alpha}, \Psi_{s\beta}, \omega_r$ are respectively the α - β rotor fluxes, the α - β stator currents and the rotor electrical speed.

The parameters $T_i, \sigma, T_s, T_r, K_r$ are defined respectively as $T_i = \frac{\sigma T_s T_r}{T_r + T_s - \sigma T_s}$, $\sigma = 1 - \frac{M^2}{L_s L_r}$, $T_s = L_s / R_s$, $T_r = L_r / R_r$, $K_r = M / L_r$, where M, L_s, L_r, R_s, R_r are respectively the magnetizing, the stator and rotor inductances, the stator and rotor resistances. L_s and L_r can be expressed as sum of the magnetizing and the leakage inductances L_{ss} and L_{sr} respectively.

The mechanical equations are:

$$\frac{d\omega_r}{dt} = \frac{p}{J}(C_e - C_r) \quad (5)$$

$$\frac{d\vartheta_{rm}}{dt} = \frac{\omega_r}{p} \quad (6)$$

with:

$$C_e = \frac{3}{2}p \frac{M}{L_s}(\Psi_{r\alpha}I_{s\beta} - \Psi_{r\beta}I_{s\alpha}) \quad (7)$$

where p is the number of poles pair, C_e and C_r are the electromagnetic and the resistive load torque respectively, J the motor-plus-load inertia, ϑ_{rm} is the rotor mechanical position.

In this model, the inductive parameters L_s, L_r and M are assumed to be constant respect to both current and rotor position variations, differently from the co-simulation approach presented in the next paragraph.

B. FEM model

The FEM model of the induction motor has been developed in ANSYS Maxwell[®]. Differently from synchronous machine, the presence of the rotor bars in IMs requires special attention. In fact, the torque is function of the time-dependent currents that flow in the rotor bars. This effect can be evaluated considering the time-varying flux linking the different rotor bars and the conductivity of the bars themselves. The variability of the rotor flux linkage depends by the variable currents flowing in the stator windings and the rotor speed.

The FEM model considers the eddy effects in the rotor bars and the presence of the end-connection region, simulating the effect of the rotor shorting ring by parameters of end-resistance and end-inductance between adjacent conductive bars. With this approach the rotor resistance varies as function of skin and proximity effect in different load conditions. The FE analysis by Maxwell[®] also permits to evaluate, for each different load condition, the motor parameters in terms of stator and rotor resistance, stator and rotor leakage inductance, and magnetizing inductance simulating the classical no-load and locked rotor tests, [15][16]. The motor parameters at the rated (base) operating conditions, calculated by FEM and used in the lumped parameters model approach (described in Section 4), are listed in TABLE II. , while the rated values are summarized in TABLE III. A FEM “transient” analysis by ANSYS Maxwell[®] is intended as a tool to evaluate the performance of a FEM simulated motor with impressed time-varying supply conditions, i.e. frequency and amplitude of the stator voltages, rotor speed or slip speed for an induction motor.

TABLE II. MOTOR PARAMETERS AT RATED CONDITIONS EVALUATED BY FEM

Motor parameters at rated conditions		
R_s	Stator resistance	0,0175 Ω
R_r	Rotor resistance related to stator side	0.0196 Ω
L_s	Stator leakage inductance of stator side	0,0478 mH
L_r	Rotor leakage inductance of stator side	0,0962 mH
M	Main inductance coupling stator and rotor	1,071 mH
p	Number of pole pairs	2
J	Moment of inertia	0,0197 kgm ²

TABLE III. RATED (R) AND BASE (B) VALUES EVALUATED BY FEM

Rated and base values	
Current (r/b)	589 A (peak)
Voltage (r/b)	337 V (peak)
Frequency (r/b)	207 Hz
Flux (b)	0.25 Wb
Torque (r)	340 Nm
Speed (r)	6000 rpm
Slip (r)	0.0339
No-load current	224 A (peak)

Fig. 2 shows the torque waveform obtained by the transient analysis at rated (sinusoidal) currents and slip conditions. The ripple oscillations due to the presence of the slots is clearly visible. Let consider that this “static” torque ripple is quite different compared to the “dynamic” one obtained by the co-simulation approach when the controller action is accounted (see Section 5).

Fig. 3 shows the distribution of the current density in the rotor bars and the flux density map at rated condition. In particular, the non-uniform distribution of current in the conductor is function of the skin effect. This effect can vary a lot in transient states and the current density values are more significant in the direction of the air gap when the frequency is high, changing consequently the equivalent bar resistance.

Thereafter, the FEM model used in this study considers the time-variation of the bars’ resistance with evident increase in accuracy respect to the lumped parameters model that uses a constant value of rotor resistance.

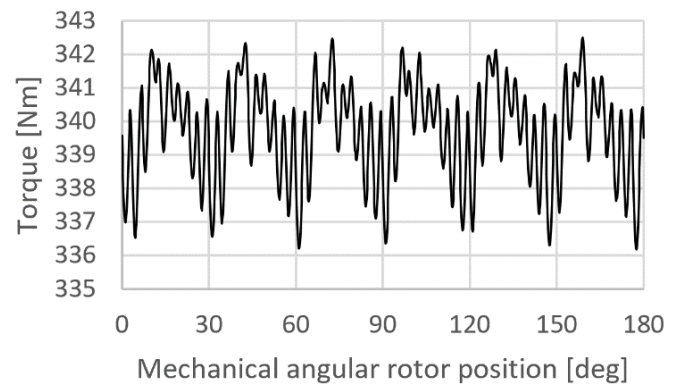


Fig. 2. Torque waveform at rated ideal supply

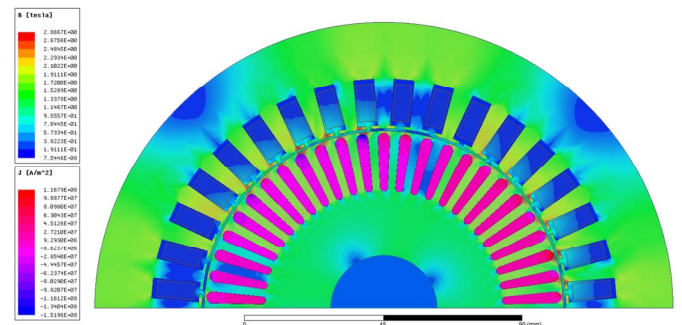


Fig. 3. Current density in the rotor bars and the flux density map at rated condition

III. CONTROL SCHEME

The control strategy considered in this study is the Field-Oriented Control (FOC), one of the most outstanding and widely used methods of vector control. FOC of IMs features high efficiency and better transient performance compared to scalar-controlled drives. Rotor Flux-Oriented Control (RFOC) is preferred for IMs, as it allows separate manipulation of machine's flux and torque and hence enables an easy and effective control similar to a DC-machine.

Its implementation requires the knowledge of the time-varying rotor flux position $\vartheta(t)$ and amplitude $\Psi_r(t)$.

By considering the equivalent IM model (lumped parameters) in the rotor-flux aligned reference frame $d-q$ we find:

$$\frac{dI_{mr}}{dt} + \frac{1}{T_r}(I_{mr} - I_{ds}) = 0 \quad (8)$$

$$\omega_2 = \frac{1}{T_r} \frac{I_{qs}}{I_{mr}} \quad (9)$$

$$\vartheta(t) = \int_{t_0}^t \omega(t) dt = \int_{t_0}^t \left(\omega_r + \frac{1}{T_r} \frac{I_{qs}}{I_{mr}} \right) dt + \vartheta(t_0) \quad (10)$$

where $I_{mr} = \Psi_r/M$ is the *rotor magnetizing current*, proportional (by definition) to the amplitude of the rotor flux: according to (8) it depends from the d-component of the stator current I_{ds} only; $\omega_2 = \omega - \omega_r$ is the *slip speed*, difference between the rotor flux (synchronous) speed ω and the rotor speed ω_r : according to (9) it depends from the q-component of the stator current I_{qs} (providing the rotor magnetizing current is constant).

Equations (8) to (10) represent the *rotor flux current model*. The only parameter that characterizes this model is the rotor time constant T_r , defined in function of motor parameters as L_r/R_r .

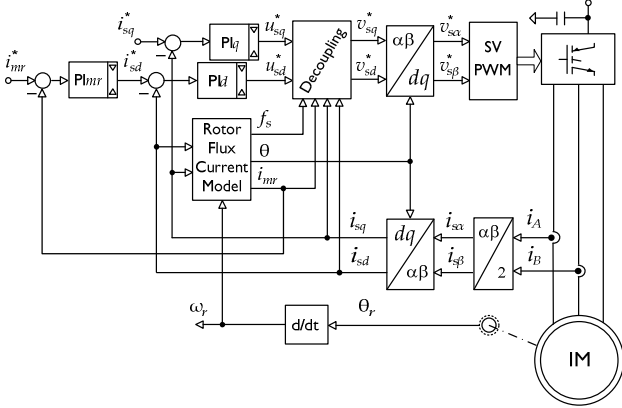


Fig. 4. Rotor flux-oriented control scheme

The control scheme of the IM based on rotor flux orientation is shown in Fig. 4. Flux and torque control are arranged by the respective d-q current components. The stator windings are fed by a current-regulated PWM voltage-source inverter. Proportional-Integral (PI) current regulators are used, with output limitation and anti-wind-up features. Their outputs represent the voltage reference of the machine. The rotor flux current model estimates the rotor flux position allowing the transformations between the stator $\alpha\beta$ and the rotor flux d-q components. It also estimates the rotor magnetizing current used in a superimposed flux regulator which provides the set-point for the d current.

As usual in vector control of IMs, the d-axis current (i.e. the rotor flux linkage) is kept constant at its rated value below the rated speed (constant-torque region), while it is reduced above the rated speed (field-weakening region) to comply with the voltage feeding limit. According to the usual practice, a decoupling block has been included at the outputs of the current regulators in order to improve the control dynamics.

The decoupling equations, expressed with per units variables, are:

$$v_{sd} = u_{sd} - x_\sigma f_s i_{sq} - \frac{x_s - x_\sigma}{\omega_b T_r} i_{mr} \quad (11)$$

$$v_{sq} = u_{sq} + x_\sigma f_s i_{sd} + (x_s - x_\sigma) f_s i_{mr} \quad (12)$$

The per unit rotor magnetizing current $i_{mr} = I_{mr}/I_b$ and synchronous frequency $f_s = \omega/\omega_b$ are calculated by the rotor flux estimator; the parameters are defined as follows: $x_s = L_s \frac{I_b}{\Psi_b}$, $x_\sigma = \left(L_s - \frac{M^2}{L_r} \right) \frac{I_b}{\Psi_b}$; $\omega_b/2\pi$, I_b , Ψ_b are the base frequency, current, and flux respectively (see TABLE III.).

An accurate knowledge of the parameters involved in the rotor flux model and in decoupling equations is necessary to precisely control the IM. However, especially the rotor parameters are difficult to measure and easy to drift (due to the temperature, eddy and saturation effects mainly). The effects of modelling mismatches outlined by the finite elements method co-simulation approach will be shown in Section 5.

IV. CO-SIMULATION STUDY SET-UP

The co-simulation scheme set for the aims of this study is shown in Fig. 5. The drive control and the ideal Space Vector PWM (SV-PWM) inverter are simulated in Simulink. The output inverter voltages are applied to both the FEM motor model running in Maxwell[®] and the LP model running in Simulink. Hence, the two models receive the same voltage inputs at each time step and provide their respective outputs, particularly the feedback variables needed for the control (phase currents and speed). Depending on the test case, the FEM model or the LP model feedbacks are used to close the control loop.

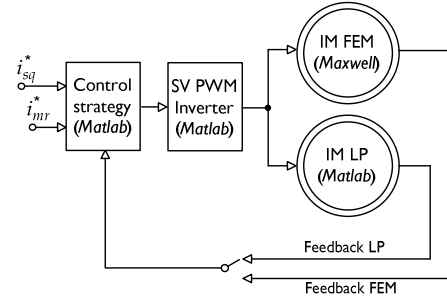


Fig. 5. Set up of the comparative study between FEM and LP models

The FEM model running in ANSYS Maxwell[®] is called through the respective interface in Simplerer (FEA1 in Fig. 6), which provides the electrical and mechanical inputs and outputs nodes for connections with the power supply and resistive load, respectively. The electrical inputs are the feeding voltages at the motor terminals, impressed with respect to the reference point 0 of the assumed voltage-source inverter (V_{10} , V_{20} , V_{30}). The motor is star-connected and the potential difference between the star centre M and the reference point is measured (V_{M0}), such as the actual phase voltages (V_{1M} , V_{2M} , V_{3M}). The mechanical system is fed by the motor torque provided by the FEM model and the resistive load torque generated in Simulink. The computed rotor speed is a time-varying input of the FEM model.

The control scheme in Simulink reproduces the structure in Fig. 4, exactly. Each block is implemented by its discrete algorithm using MATLAB Functions. The SV-PWM algorithm saturates the feeding voltage at the rated value, in order to verify the rated performance. The algorithm maintains, at each time step in saturation, the phase of the reference voltage space vector. To avoid effects of control delays, not within the scopes of this study, sampling time and PWM periods are set identical and equal to the fixed time-step of the simulation solvers. The ideal inverter feeds the motor models (both LP and FEM models) by the “mean-in-the-PWM-period” voltages computed by the SV-PWM algorithm. Considering this model of modulator-inverter pair, the regulators reference values have to take into account the voltage limit imposing by the DC bus and the modulation holding time. The LP model is implemented by a Differential Equations Editor (DEE) block in Simulink, while the FEM model is linked through the Sim2Sim interface.

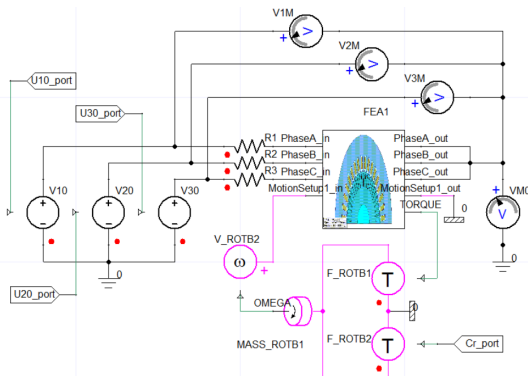


Fig. 6. FEM model interface and feeding scheme in ANSYS Simplorer®

V. RESULTS AND COMPARISONS

An exhaustive test case is simulated for the IM drive. It includes an initial magnetization period followed by a speed transient toward rated speed and load torque conditions. The magnetization is generated by a step variation of the flux d-current reference at $t = 0.5$ ms; the speed transient follows the step variation of the torque q current reference at $t = 40$ ms; while the steady-state operation is forced by the (rated) voltage saturation, for that constant rated speed is expected after rated load application. To minimize the simulation time both the magnetization and the speed transient are arranged to be as fast as possible, compatibly with the rated current: magnetization is driven by the rated motor current, the load inertia is set to zero, and the load torque is applied (with a smooth 2nd order dynamics) when the speed is approaching its rated value at $t = 80$ ms. With these tricks, the whole test corresponded to 140 ms of operation.

The same time-step size has been used for the solvers' algorithms in Simulink and Simplorer, equal to 20 μ s, which proved to be a good compromise between accuracy and calculation time. The resulting simulation time was about 1 h and 43 min on a computer with INTEL® Core™ i7- 6700 CPU 3.40 Ghz, 16 GB of RAM. For the sake of comparison, the same test with the LP model only (bottom connection of the switch in Fig. 5) required about 12 s.

A. LP model closed in control loop

The results when the LP model is used to close the control loop are presented in Fig. 7 and Fig. 8. After the fast magnetization at rated current, Fig. 7, the flux d-current attains the no-load rated value at about 25 ms, driven by the superimposed rotor magnetizing current regulator. Then the (rated) torque q-current reference is applied at 40 ms, which causes a current controlled speed transient (without load torque). The speed increases up to a value a little above the rated speed, Fig. 8, when the voltage saturation is attained: from here on, current control is lost. When the load torque is applied, steady state operation at rated conditions is achieved (see TABLE III.). While the response of the LP model matches exactly the control action, the torque waveform of the FEM model exhibits large oscillations during the speed transient, and it is affected by an evident ripple. The torque ripple mainly depends on the saturation phenomena considered by the FEM model. To outline this aspect, the phase currents and flux linkages computed by the FEM model are shown in Fig. 9 and Fig. 10. A non-negligible homopolar flux component is present, which slightly increases by the current, a clear effect of the saturation and the distortion current waveform, [17]. The relation between this effect and the torque ripple is shown in Fig. 11: the ripple has twice the frequency of the homopolar flux component. We also notice that the ripple amplitude, equal to about the 7% of the rated torque, is larger than that computed by the ideal rated supply in Fig. 2. Finally, there are no obvious effects of the stator slots on the ripple, although the time step-size used in the simulation provides a resolution capable to highlighting them (0.72 mechanical degrees at 6000 rpm).

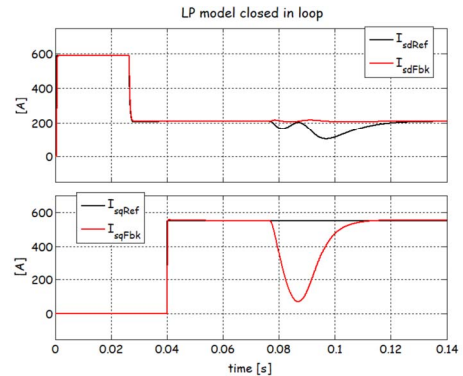


Fig. 7. Current control waveforms with the LP model closed in control loop.

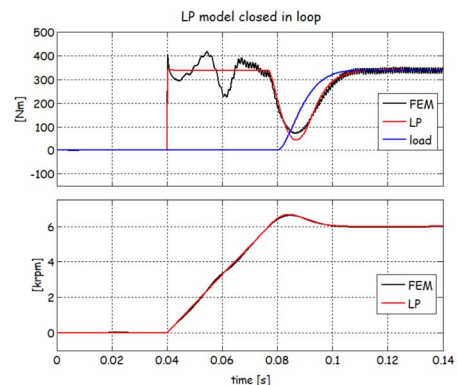


Fig. 8. Torque and speed waveforms with the LP model closed in control loop.

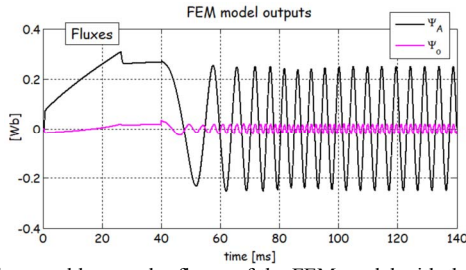


Fig. 9. Phase and homopolar fluxes of the FEM model with the LP model closed in control loop.

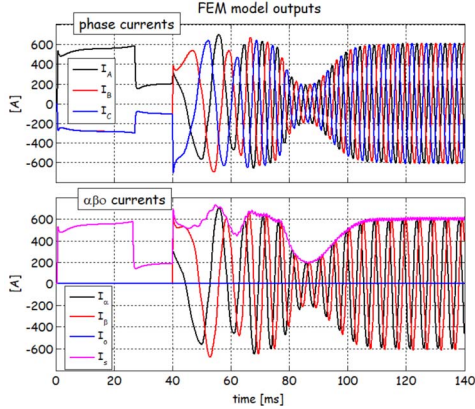


Fig. 10. Currents of the FEM model with the LP model closed in control loop.

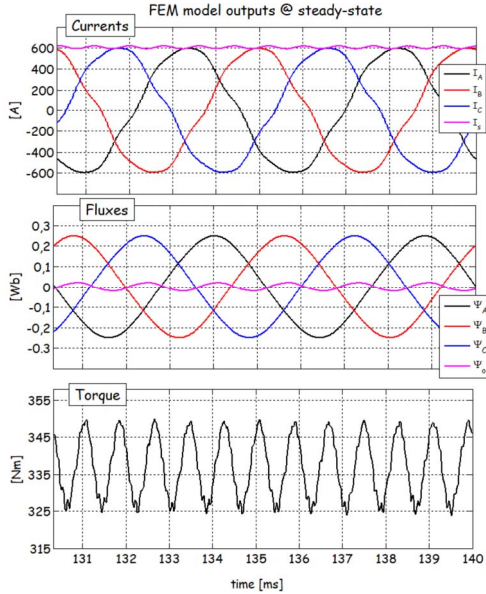


Fig. 11. FEM model outputs at steady-state with the LP model closed in control loop.

B. FEM model closed in control loop

The results in the opposite case when the FEM model closes the control loop are presented from Fig. 12 to Fig. 16. Current control feedbacks and references are shown in Fig. 12. Behaviours resemble those of the previous case, although with an evident ripple in the feedbacks. Let notice that such ripple is present also in the flux current reference, as it depends on the outer rotor-magnetizing current loop. Now, it is the FEM model which globally matches the control action but with some detuning evidences. In fact, when the speed increases in Fig. 13, the FEM model exhibits a slight but evident torque reduction due to incorrect decoupling (in fact, decoupling

equations and rotor flux model are based on LP model). Moreover, the rated conditions of TABLE III. are not attained at steady state when the FEM model is closed in control loop, since the speed reaches about 5630 rpm, 6% less than the expected rated value. In fact, the synchronous speed estimation is still based on the constant parameters flux model and does not match the FEM model behaviour during transients, i.e. when the machine is far from the conditions which match those parameters. Then, according to equation (10), an estimation error accumulates which leads to a steady-state frequency of 195 Hz, that is about the 6% less than the rated one. It is useful to underline that an increase of the saturation voltage of the 6% above the rated one allows the rated torque/speed operation with the controlled FEM model too.

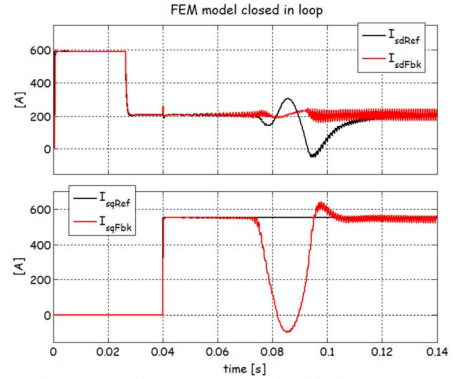


Fig. 12. Rotor-flux oriented current control with the FEM model closed in control loop.

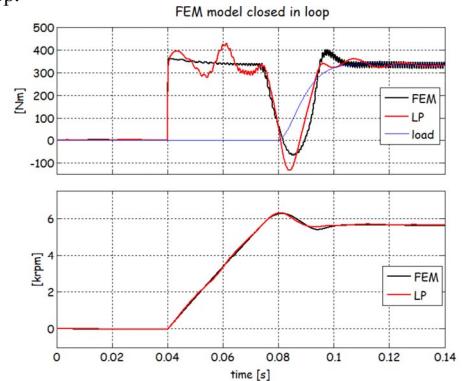


Fig. 13. Torque and speed waveforms with the FEM model closed in control loop.

The FEM model outputs overall behaviours reflect those obtained when the LP model is on-line. The dependence of the homopolar flux component by the current is now clearly evident by the comparison of Fig. 14 and Fig. 15. The distortion of the phase currents at steady-state (when the machine is fed by sinusoidal voltages in voltage saturation condition) is clear. Marginal differences in torque average value and ripple can be detected in Fig. 16.

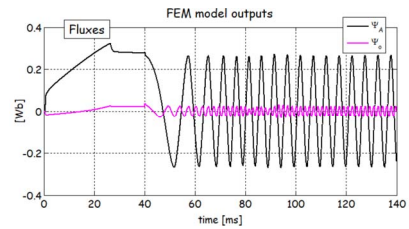


Fig. 14. Phase and homopolar fluxes of the FEM model closed in control loop.

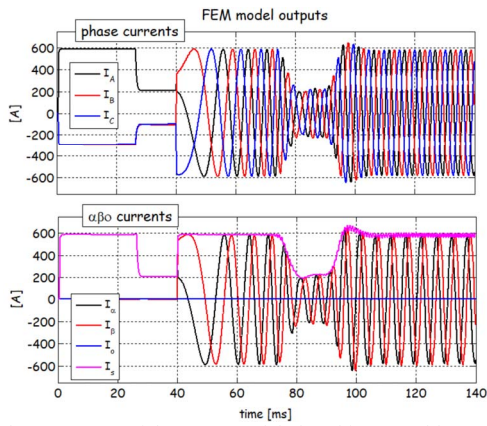


Fig. 15. Phase currents of the FEM model closed in control loop.

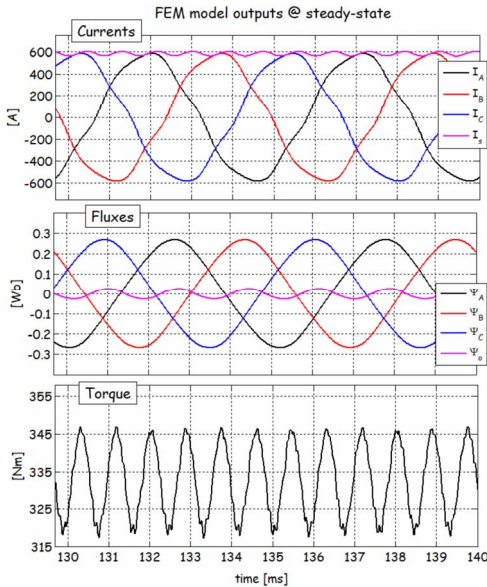


Fig. 16. FEM model outputs at steady-state with the FEM model closed in control loop.

VI. CONCLUSIONS

This paper presents the finite elements model co-simulation of a 200kW induction motor designed for the traction of a high class EV. The study highlights the presence of torque ripple due to saturation and the effect of the controller's detuning for the correct prediction of the supply rated requirements. A lumped parameters model is derived by FEM in rated conditions and used to design the control strategy parameters. When rotor flux orientation and decoupling, based on these parameters, are employed and the motor is modelled by its FEM model in co-simulation (instead of the lumped parameters model), controller detuning has been verified, which leads to about 6% of underestimation of the voltage requirement. Let notice that this aspect cannot be evaluated without the finite elements model co-simulation approach. Future study will use the co-simulation approach for the set-up of flux models closer to the actual machine behaviour.

ACKNOWLEDGMENT

This project has received funding from the European Union's Horizon 2020 Research and Innovation Programme under the Grant Agreement No 770143.

REFERENCES

- [1] D. Dorrell, A. Knight, L. Evans and M. Popescu, "Analysis and Design Techniques Applied to Hybrid Vehicle Drive Machines—Assessment of Alternative IPM and Induction Motor Topologies," *IEEE Transactions on Industrial Electronics*, vol. 59, no. 10, pp. 3690-3699, 2012.
- [2] Stumper, A. Dotlinger and R. Kennel, "Loss Minimization of Induction Machines in Dynamic Operation," *IEEE Transactions on Energy Conversion*, vol. 28, no. 3, pp. 726-735, 2013.
- [3] G. Pellegrino, A. Vagati, B. Boazzo and P. Guglielmi, "Comparison of Induction and PM Synchronous Motor Drives for EV Application Including Design Examples," *IEEE Transactions on Industry Applications*, vol. 48, no. 6, pp. 2322-2332, 2012.
- [4] Credo, A., Fabri, G., Villani, M. and Popescu, M. (2019). High Speed Synchronous Reluctance Motors for Electric Vehicles: a Focus on Rotor Mechanical Design. 2019 IEEE International Electric Machines & Drives Conference (IEMDC).
- [5] M. Villani, M. Tursini, M. Popescu, G. Fabri, A. Credo and L. Di Leonardo, "Experimental Comparison Between Induction and Synchronous Reluctance Motor-Drives," *2018 XIII International Conference on Electrical Machines (ICEM)*, 2018.
- [6] J. Holtz and N. Oikonomou, "Fast Dynamic Control of Medium Voltage Drives Operating at Very Low Switching Frequency—An Overview," *IEEE Transactions on Industrial Electronics*, vol. 55, no. 3, pp. 1005-1013, 2008.
- [7] A. Alexandridis, G. Konstantopoulos and Q. Zhong, "Advanced Integrated Modeling and Analysis for Adjustable Speed Drives of Induction Motors Operating With Minimum Losses," *IEEE Transactions on Energy Conversion*, vol. 30, no. 3, pp. 1237-1246, 2015.
- [8] D.W. Novotny, T.A. Lipo, Vector Control and Dynamics of AC Drives, Oxford University Press Inc., 1996.
- [9] N. Bianchi, S. Bolognani and G. Comelato, "Finite element analysis of three-phase induction motors: comparison of two different approaches," *IEEE Transactions on Energy Conversion*, vol. 14, no. 4, pp. 1523-1528, 1999.
- [10] L. Di Leonardo, F. Parasiliti, M. Tursini, M. Villani, "Transient Analysis of PM Synchronous Motor Drives by Finite Element Model co-Simulation," *IECON 2013 Vienna Nov. 2013*, pp. 6834-6840.
- [11] A. Gazdac, L. Di Leonardo, A. Mpanda Mabwe, F. Betin and M. Villani, "Electric circuit parameters identification and control strategy of dual-rotor Permanent Magnet Induction Machine," *2013 International Electric Machines & Drives Conference*, 2013.
- [12] C.M. Apostoaia, "AC Machines and Drives Simulation Platform," *IEMDC 2013 - IEEE International Electric Machines and Drives Conference*, Chicago, IL, May 12-15, 2013.
- [13] M. Tursini, L. Di Leonardo, A. Di Tullio and E. Della Loggia, "Transient analysis of multiphase PM motor-drives by non-linear modeling," *2016 International Symposium on Power Electronics, Electrical Drives, Automation and Motion (SPEEDAM)*, 2016.
- [14] Riviere, N., Volpe, G., Villani, M., Fabri, G., Di Leonardo, L. and Popescu, M. (2019). Design Analysis of a High Speed Copper Rotor Induction Motor for a Traction Application. 2019 IEEE International Electric Machines & Drives Conference (IEMDC).
- [15] S. Shaw and S. Leeb, "Identification of induction motor parameters from transient stator current measurements," *IEEE Trans. on Industrial Electronics*, vol. 46, no. 1, pp. 139-149, 1999.
- [16] A. Del Gobbo, F. Parasiliti, and M. Tursini, "Microcontroller-Based On-Line Self-Tuning of the Rotor Time Constant for Field-Oriented Induction Motor Drives," *Proc. of IEEE Int. Symp. on Industrial Electronics (ISIE)*, Guimaraes, Portugal, July 7-11, 1997, Vol. 3, pp. 1044-1049.
- [17] Ferreira, F., Silva, A., Cruz, S. and De Almeida, A. (2017). Comparison of losses in star- and delta-connected induction motors with saturated core. 2017 IEEE International Electric Machines and Drives Conference (IEMDC).